Proceedings of the 2014 Joint Rail Conference
JRC2014
April 2-4, 2014, Colorado Springs, CO, USA

JRC2014-3763

A SPATIAL GEOMETRY APPROACH TO VARIABLE CROSS-SECTION RAIL MODELING: APPLICATION TO SWITCHES AND TURNOUTS

Martin B. Hamper
Department of Mechanical and Industrial Engineering
University of Illinois at Chicago
Chicago, IL 60607, USA

Conrad Ruppert, Jr.
Department of Civil and Environmental Engineering
University of Illinois at Urbana-Champaign
Urbana, IL 61801, USA

Cheng Wei
Department of Aerospace Engineering
Harbin Institute of Technology
Harbin, Heilongjiang, 150001, China

Ahmed A. Shabana
Department of Mechanical and Industrial Engineering
University of Illinois at Chicago
Chicago, IL 60607, USA

ABSTRACT

Contact between the wheel and rail can have a significant effect on the dynamics of vehicle/track interaction models. Many existing rail surface models rely on curve based geometry which may lead to some geometric inaccuracy in the case of variable cross-section rails. This investigation will focus on the development of a new spatial geometry based rail surface description which reduces this geometric inaccuracy. It has been shown in literature that certain CAD geometry types, such as B-Spline curves and surfaces, may be converted to equivalent *absolute nodal coordinate formulation* (ANCF) finite elements without a loss of geometric accuracy. To this end, a new ANCF surface description of variable cross-section rails is developed. This investigation also demonstrates the feasibility of using, in the future, 3D surface scanning techniques as well as profile curve measurements to develop a rail surface geometry model using the new ANCF surface which can be systematically integrated with complex *multibody system* (MBS) models. A realistic railroad vehicle example of a turnout, which includes variable cross-section rails, is tested for the case of the new ANCF surface. A study of the numerical results reveals the benefits of using the ANCF surface geometry developed in this investigation.

1. INTRODUCTION

In the analysis of railroad vehicle system dynamics, contact between the wheel and rail is a fundamental feature in any realistic model. To this end, many methods have been introduced which rely on curve geometry to represent the contact surfaces such as the curve network representation [12]. In this technique, the profile curve of the rail surface is swept along a space curve which represents the centerline of the rail. It has been shown that this method is viable in the case where the profile of the rail is constant; however it is insufficient for rail sections that have geometry which varies along the rail space curve. A number of approaches have been introduced in literature to produce a geometric approximation of the variable cross-section rail surfaces. The bulk of these methods rely on direct interpolation of a series of rail profile curves. This procedure is well suited for the case in which off-line tabular contact procedures are employed. However when on-line non-linear contact evaluation procedures are employed, such as those presented by Shabana et al.[12], a poor description of the wheel/rail interaction forces is produced. Recently, Hamper et al. [4] presented a new surface based description of the rail surfaces which alleviates this issue. It is the main objective of this investigation to elaborate on how this technique may be integrated with modern virtual prototyping and measurement tools.

In off-line contact search methods, a significant amount of work is performed at a pre-processing stage to determine the location of a contact point under a limited range of scenarios. This data is then compiled in tabular form as a function of a small set of parameters which are interpolated at runtime to determine the location of the contact point as well as other parameters required to determine the contact forces. Due to the complexity of the problems, these tables are often formed under

the assumption that one rail is fully constrained to the ground. One such method is that applied by Kassa et al. [6] in which a contact table is formed to solve the wheel/rail contact problem of variable cross-section rails. A similar approach is presented by Alfi and Bruni [1]. Sugiyama et al. [18] employed a procedure in which the derivatives of the profile curves, which are described using three-layer splines, are also computed via linear interpolation of two adjacent profiles. Kassa et al. uses the distance traveled along the rail and the lateral shift of the vehicle to define a set of tabular contact functions which contain the information necessary to define the location and forces associated with the wheel/rail contact. Linear interpolation between these contact functions is performed at runtime with some success as is demonstrated by Kassa and Nielsen [7] where a series of tests were performed to compare measured and numerical results. It is important to note that many tabular based contact evaluation methods do not account for relative rotations between the wheel and rail. In many scenarios this approximation is sufficient as is demonstrated by the validation presented in the literature [7], however this assumption is only valid provided that the relative rotations remain small.

In on-line contact search methods, computational geometry (CG) methods are employed at runtime to determine the location of a contact point. Additional parameters are often computed in order to determine the associated wheel/rail interaction forces. Many authors have made use of curve geometry for the on-line contact problem with some success. For example, Schupp et al. [11] presented a method in which linear interpolation between two adjacent profiles is used at runtime to determine an intermediate profile of the rail at the current location. Wan et al. [19] presented a method of reducing the three dimensional problem to a two dimensional case in which only the distance along the trajectory curve and vertical height of the rail profiles are considered. The common feature of these approaches is the use of curve geometry to represent three dimensional surfaces. As with the tabular approach, this method is successful over a range of scenarios but cannot capture the full range of features available in surface based geometric methods.

Since the contact problem is highly non-linear, the off-line approach has a advantage in computation time; however this method is limited to the range of scenarios calculated at the pre-processing stage, giving the on-line approach a advantage in robustness. However, there exists an additional limitation in the direct profile curve interpolation method presented by Schupp et al. [11] when employed in conjunction with either the three dimensional non-conformal elastic or constraint contact approaches [12]. As was discussed by Sinokrot et al. [15], the elastic contact approach requires second order spatial derivative continuity (C^2) of the wheel and rail surfaces while the constraint contact approach requires third order derivative continuity (C^3). Clearly a surface created via linear interpolation using more than two profile curves will have a discontinuity in the first order derivatives at the location of each interior profile, thus the surface has only position level continuity (C^0). A direct consequence of this, as will be shown in the numerical results of this investigation, is a fictitious spike in the predicted contact forces at the location of the spatial derivative discontinuity. It is for this reason that a new technique was developed to model variable cross-section surfaces without the need for direct interpolation between profiles when the on-line approach is employed.

Rather than using the curve based approach previously discussed, the new technique developed relies on the construction of a surface at a pre-processing stage using a mesh of *absolute nodal coordinate formulation* (ANCF) thin plate elements which employ bi-quintic interpolation [4]. It was shown by Hamper et al. that under the appropriate circumstances, which will be discussed in this investigation, a surface created using these elements has continuity. The most direct approach to generating a surface of ANCF thin plate elements begins with constructing a B-spline surface which may be converted into a collection of ANCF thin plate elements without any loss of geometric accuracy using the technique discussed by [4, 8, 9]. Due to the fact that B-spline surfaces may employ a very fine discretization, this conversion may also be applied by direct evaluation of the position and spatial derivatives of the B-spline surface to generate the ANCF nodal coordinates. This provides the option for the user to select a smaller subset of the potential ANCF nodes thereby producing a more coarse mesh than is generated by direct transformation from B-spline to ANCF. The following sections of this investigation will present methods which may be used to construct an ANCF surface model of variable cross-section rails using data generated by modern measurement and virtual prototyping technologies.

This paper is structured as follows: the ANCF representation of a surface is reviewed in Section 2; a discussion of surfaces created using profile curves generated by either measurement or virtual prototyping is presented in Section 3, a discussion of a procedure with which an ANCF surface may be constructed using measured data from 3D scanning devices is provided in Section 4; a numerical example of a vehicle negotiating the tangential route of a turnout is presented in Section 5 with results from the cases in which the rail contact surface is generated via linear profile interpolation and ANCF geometry being compared to demonstrate the benefits of the ANCF surface based geometry; and a summary of the conclusions drawn in this investigation are presented in Section 6..

2. ANCF SURFACES

Typically, ANCF finite elements are employed to model a continuum material [14], however the robust geometric properties of these elements lend themselves easily to the description of arbitrary curves and surfaces. Similar to

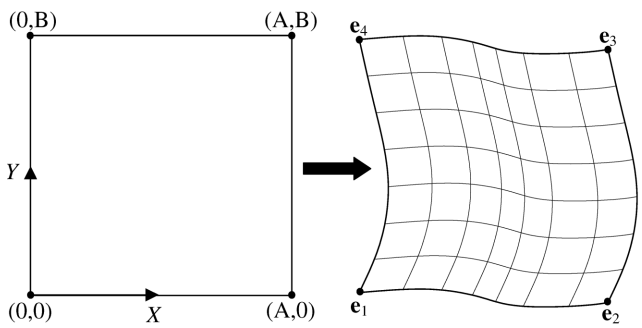

Figure 1. ANCF Thin Plate Element in Parametric (left) and Physical (Right) Domains

conventional finite elements, interpolation within the element is performed by making use of a set of nodal coordinates and polynomial shape functions which map an undeformed or reference configuration to a deformed or physical configuration as shown in Fig. 1. This relationship is defined algebraically by $\mathbf{r} = \mathbf{S}(\xi,\eta)\mathbf{e}$, where $\mathbf{r}$ is the position of a point in an element, $\mathbf{S}$ is the matrix of shape functions, $\mathbf{e}$ is the vector of nodal coordinates, and ξ and η are the coordinates of the reference domain. In the case of a rigid surface modeled with ANCF thin plate elements, the configuration of the rail surface does not change with time and takes the physical configuration at the initial time step. In this case, the reference configuration represents a parametric domain in which two surface parameters, defined as s_1 and s_2, are used to identify a specific point on the surface mesh. Unlike conventional finite elements, however, ANCF elements make use of both position and a collection of spatial derivative vectors to define the coordinates at each node. This allows ANCF elements to be developed which have an arbitrary polynomial interpolation order provided the correct nodal coordinates are chosen.

In the modeling of the rail surface for the contact problem, it is important to have fine control over the polynomial interpolation order as different contact formulations require different levels of spatial derivative continuity. For example, the on-line three-dimensional non-conformal elastic contact formulation employed in this investigation, denoted as the *elastic contact formulation - algebraic equations* (ECF-A), has been shown to require continuity in the spatial derivatives up to the second order by Sinokrot et al. [15]. Therefore, Hamper et al. [4] developed an ANCF thin plate element which satisfies this condition throughout the entire rail surface mesh. This element, shown in Fig. 1, is a four node quadrilateral which employs bi-quintic interpolation and requires nine coordinate vectors at each node. These coordinate vectors include the position and all mixed partial spatial derivatives up to the second order with respect to both the *X* and *Y* coordinates. It was demonstrated by Hamper et al. [4] that the second order spatial derivative continuity is satisfied in only the case where the reference configuration of the mesh forms a rectangular grid, meaning all elements in a row have the same

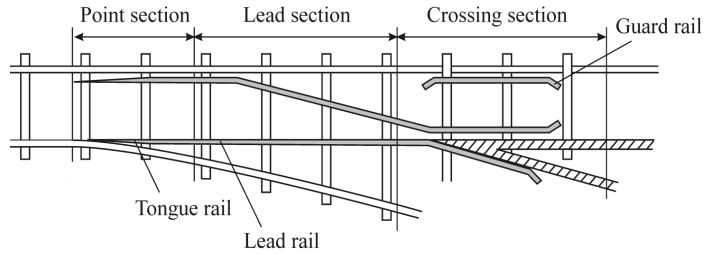

Figure 2. Right Hand Turnout Diagram [12]

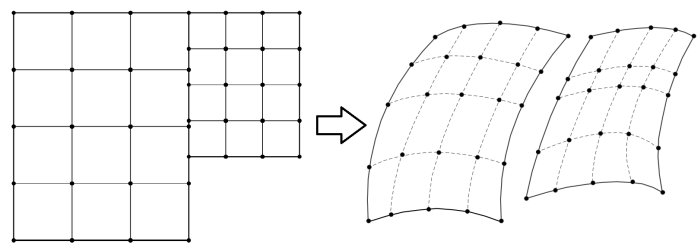
Figure 3. ANCF Thin Plate Mesh With Physical Discontinuity (Left: Reference Domain, Right: Physical Domain)

height and all elements in a column have the same width. Considering that it is the physical configuration which takes the shape of the rail surface and not the reference configuration, it is a trivial matter to ensure this condition is satisfied for a rail which has a variable cross-section.

The physical geometry of a rail surface need not be continuous in the general case. Take for example a turnout, as is shown in Fig. 2, which is composed of multiple rail segments which have physical discontinuities between them. However, ECF-A may suffer from numerical instabilities when the reference domain is discontinuous. It would be inappropriate to model the surface at the interface between two of these segments with position or spatial derivative continuity. To insert physical discontinuity into an otherwise continuous mesh, the rail surface may be generated from multiple rectangular grids which are joined only in the reference domain. In other words, the rectangular grids would share no nodes or elements in common, however the reference domains of the two grids would share a common boundary along the direction of one of the surface parameters thus allowing a continuous description in the reference domain. An example of this configuration is provided in Fig. 3 in which two rectangular grids have been combined in a single mesh with a common boundary along the longitudinal direction. Using this approach, one may generate a variety of rail surfaces which are composed of multiple consecutive rectangular grids which have a physical discontinuity at the boundaries in the physical domain while retaining positional continuity at the boundaries in the reference domain.

3. MINIPROF/VIRTUAL PROTOTYPING TECHNOLOGY

In this section, two methods with which a rail surface may be constructed using profile curves are considered. The first procedure, which is similar to that presented by Schupp et

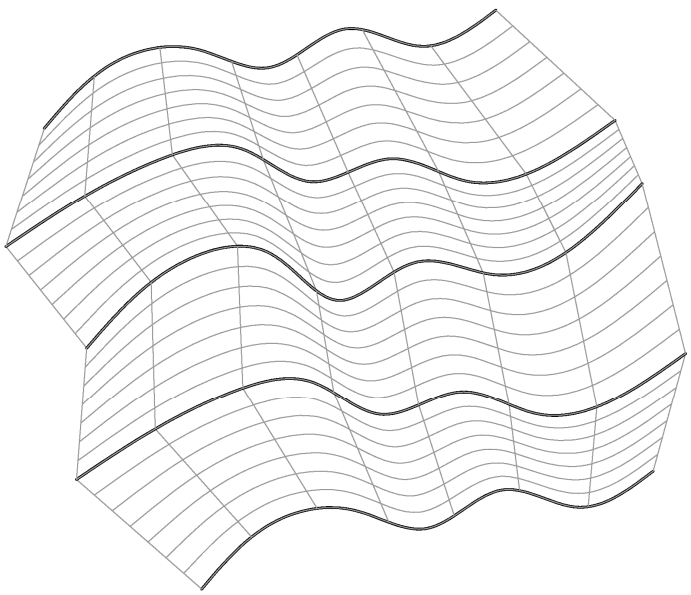

Figure 4. Linear Profile Interpolation Surface

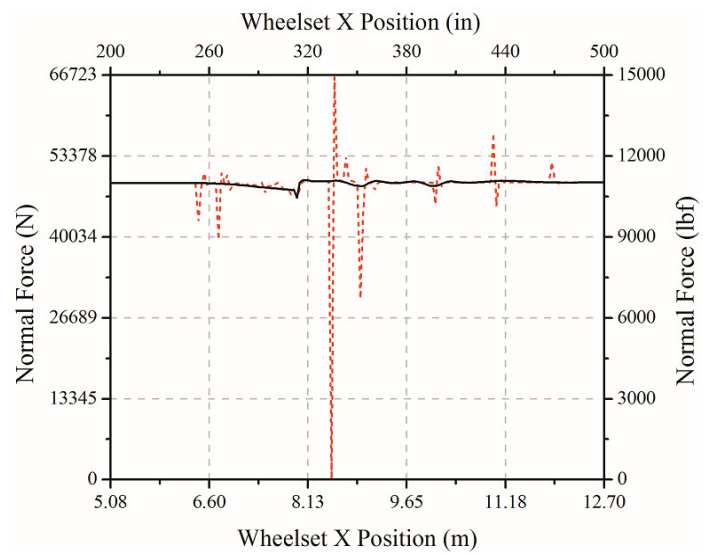

Figure 5. Normal Force at Left Contact Linear Interpolation Vs. Quintic Plate
(_ _ _ _ Linear Interpolation, _____ Quintic Plate)

al. [11], involves making use of direct linear interpolation between profile curves of the rail to generate a model of the rail's surfaces. This procedure will be referred to as linear profile curve interpolation. The second procedure, which is similar to the procedure presented by Piegl and Tiller [10], makes use of non-linear interpolation between a series of profile curves to develop a surface model. This procedure will be referred to as lofting. The benefit of choosing either of these two methods is primarily based on the lack of restriction on the source data. Rail profile curves may be measured directly using modern technology such as MINIPROF systems, or they may be generated using computer aided drafting (CAD) systems. The use of measured data is ideal for the case where a simulation is focused on the vehicle/track interaction of a physical rail system, this would be highly effective if employed in accident investigation simulations involving derailments at turnouts or crossings. The use of profile curves generated via CAD systems would be of less value in this case, however it would be a highly effective tool for the virtual prototyping process for new wheel or rail designs.

There are two primary differences between the two methods. First, in the linear profile curve interpolation method, all interpolations are performed between only two profile curves while in the lofting procedure a global interpolation is performed over the entire set of profile curves provided. The second, and more important distinction, is that while the linear profile curve interpolation method is limited to linear interpolation between profile curves, the lofting procedure allows for the use of arbitrary order polynomial interpolation to be employed. This difference can become quite significant when spatial derivative continuity requirements are imposed on the surface to be generated. It is clear that the linear profile interpolation procedure cannot guarantee continuity in any longitudinal spatial derivatives, thus this method is a poor choice for a contact formulation, such as ECF-A, which requires continuity in the second order spatial derivatives. The lofting procedure, however, does not suffer this limitation as the interpolations may be performed using an arbitrary polynomial order.

In the linear profile curve interpolation method, individual profile curves are often modeled with cubic interpolation, while the surface between two of these profiles is modeled using a linear interpolation scheme. An example of a generic surface created using this procedure is shown in Fig. 4. This figure illuminates the primary limitation which arises from the use of this procedure. As was previously discussed, the discontinuity in the longitudinal spatial derivatives as can be seen by the sharp corners produced at the location of the internal profile curves. This type of discontinuity can in turn effect the prediction of the contact forces. Take for example a suspended wheelset traveling along the tangential route of a turnout which is modeled using the linear profile curve interpolation procedure while the contact is modeled with ECF-A. Figure 5 shows the predicted normal contact force as a function of the wheelset distance, note the large spikes in this figure. The majority of these spikes directly coincide with the location of intermediate profile curves. These spikes are directly caused by the spatial derivative discontinuity caused by the use of the linear interpolation. From this, it is clear that this model of the rail surface should not be employed using similar contact evaluation procedures. The linear profile curve interpolation method is best employed when off-line tabular approaches to contact evaluation are employed, such as those found in the work of Kassa et al. [6, 7] or Alfi and Bruni [1]. This contact evaluation approach does not necessarily require continuity of the spatial derivatives of the rail surfaces, and consequently

may not suffer from the same spikes in the predicted contact forces.

4. 3D SURFACES SCANNING TECHNIQUES

3D scanning technology has recently become one of the most popular data acquisition techniques where it is necessary to construct surface models in a wide variety of applications including medical, geological, and robotics. The data extracted from these devices are often referred to as point clouds, which are a set of 3D data points taken with high enough density such that they offer an accurate approximation to the shape of the surface. An example of a point cloud is shown in Fig. 6, where a point cloud describing a turnout is generated using a combination of CG methods and a random number generator. Hieu et al. [5] made use of point cloud data from 3D scanning devices to reconstruct the surfaces of a variety of different biological components including damaged skulls, teeth, and hip joints to assist in the development of various patient specific medical implants. Slob and Hack [17] employed surface scanning and reconstruction techniques to develop highly accurate surface models of a variety of different terrain and demonstrated the ability to generate large-scale topographic maps using these techniques. Cole and Newman [2] were able to use real time 3D surface scanning to allow an autonomous robot to navigate outdoor terrain with some success. In part, these developments are due to the increasing commercial availability of 3D surface scanning devices ranging from the stationary mounted variety to hand-held devices which one may use outdoors. Notable devices in this category include the Creaform Handyscan 3D, Nikon Metrology's ModelMaker, and the Polhemus FastScan. These are highly portable handheld 3D scanning devices which may be employed to measure surface geometry in much greater detail than profile curve measurement devices allow as the density of the measured points is significantly greater than would be practical with profile curve measurement. The measurement accuracy of most devices is high enough for rail applications, for example the Handyscan 3D may take measurements with a resolution of up to 0.002 in. (0.0508 mm). Of course, these devices must be tested for this specific application before their use can be recommended for the case of track measurement.

While the resolution of 3D surface scanning devices is much greater than that of profile curve measurement, surface reconstruction from the point cloud data generated by these devices is much more complicated. There exists in literature many publications which detail various methods of surface reconstruction. According to Gálvez and Iglesias [3], these typically fall into one of three categories: polygonal meshing, constructive solid geometry (CSG), and free-form parametric surfaces. Polygonal meshing involves the generation of surfaces by drawing lines between data points and constructing polygons from the generated lines. This results in spatial derivative discontinuities so this method is not considered in this paper. The CSG approach involves taking simple primitive objects and

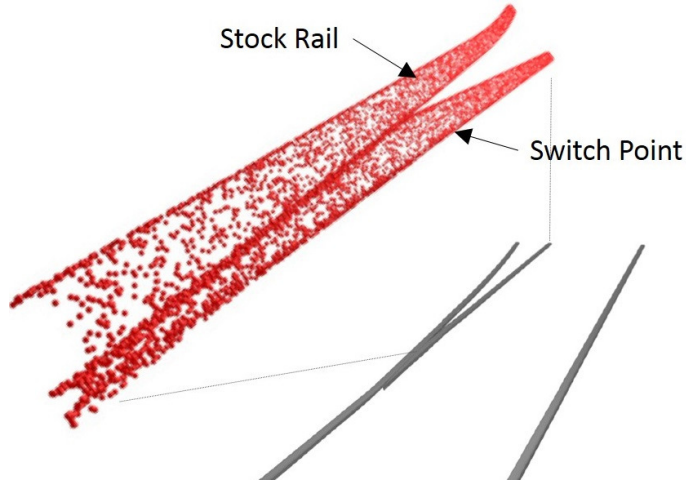

Figure 6. Point Cloud Data for a Left Hand Turnout

employing Boolean addition/subtraction operations to construct a surface. It would require undue effort to maintain the appropriate spatial derivative continuity using this approach and this is also not considered. The free-form parametric surface approach, however, is well suited to the topic of this paper as surfaces of this type may be generated with arbitrary spatial derivative continuity. Geometric definitions of this type, such as B-Spline or NURBS, are the most widely used of this type and are often employed in commercial CAD systems.

Gálvez and Iglesias [3] also present an excellent survey of the current state of the art in methods of scattered data (point cloud) surface reconstruction. Following this, the authors present a new technique which may be used to recover NURBS type surface geometry from scattered point data, such as that measured by a 3D scanner. One may easily use this technique to develop a NURBS surface from which ANCF nodal coordinates may be extracted with ease using software packages such as SISL [16]. It is the opinion of the authors that this procedure may be implemented without difficulty thus allowing for the construction of variable cross-section rail surfaces for use in dynamic vehicle/track interaction simulations.

5. NUMERICAL EXAMPLE

In this section, a simple example is presented to demonstrate the techniques discussed in this work. A suspended wheelset traveling at a constant velocity over a partial left hand turnout is chosen as an idealized scenario in which a railroad vehicle may encounter a rail with a variable profile. The numerical simulations are carried out for three different scenarios that correspond to the three surface types: linear interpolation, an existing cubic ANCF thin plate, and the newer quintic ANCF thin plate. The results obtained using the three different surfaces are compared. The simulations are carried out using the general purpose multibody package SAMS/2000 [13].

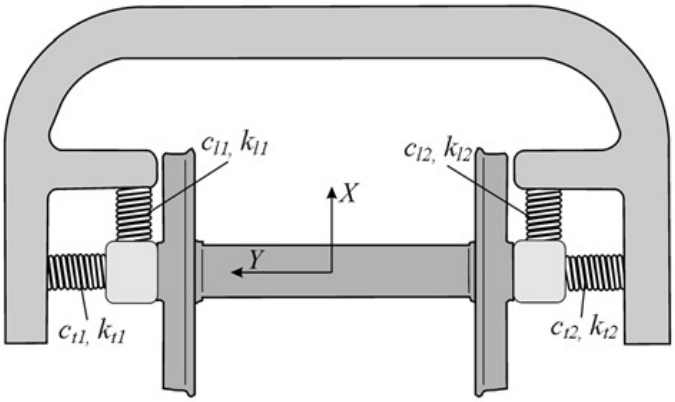

Figure 7. Suspended Wheelset

5.1 Simulation Parameters

The suspended wheelset used in this example is composed of a single wheelset and a frame connected by linear spring-damper elements as is shown in Fig. 7. The stiffness and damping of the suspension components are defined as $k_{l1} = k_{l2} = 14$ kN/m (925 lbf/ft), $k_{t1} = k_{t2} = 25$ kN/m (1713 lbf/ft), $c_{l1} = c_{l2} = 1$ kN·s/m (68.5 lbf·s/ft), and $c_{t1} = c_{t2} = 1$ kN·s/m (68.5 lbf·s/ft). A constant velocity constraint is applied to the frame with a value of 4.47 m/s (10 mph) to simulate the vehicle motion while an axle load of 98 kN (22,000 lbs) is applied to the wheelset to simulate the vehicle weight. The frame has a mass of 10,000 kg (685.2 slug), with roll, pitch, and yaw mass moments of inertia defined as 1,799.03, 1,799.03, and 2,499.96 kg·m^2 (1,326.9, 1,326.9, and 1,807.0 slug·ft^2) respectively; while the wheelset has a mass of 1,567.39 kg (107.4 slug), with roll, pitch, and yaw mass moments of inertia defined as 655.94, 167.99, and 655.94 kg·m^2 (483.8, 123.9, and 483.8 slug·ft^2) respectively. The wheel profile used in the example is the AAR-1B-WF which is positioned such that a flange clearance of 0.73914 cm (0.291 inches) is maintained in the equilibrium position.

A partial turnout is considered for the track model; the components included are the left and right stock rails, the left switch point and lead rail. For simplicity of the analysis, the guard, frog, and right switch point sections are not included in the model. Each of the three geometric models is created from the same set of rail profiles. The left rail is modeled using 36 profiles for the stock rail and 28 profiles for the tongue and lead rails while the right rail is modeled using 36 profiles. These profiles were developed based on CAD drawings provided by Cleveland Track Materials (CTM). The stock profile of the rail used in this model is the 136 RE, while the tongue and lead rails belong to a No. 9 left hand turnout typically used in yards with a maximum speed rating of 6.67 m/s (15 mph). The rails are positioned such that the track gage is 1.4351 m (56.5 inches) and the switch point is located at 6.858 (270 inches) along the left stock rail.

The linear interpolation surface is generated by direct

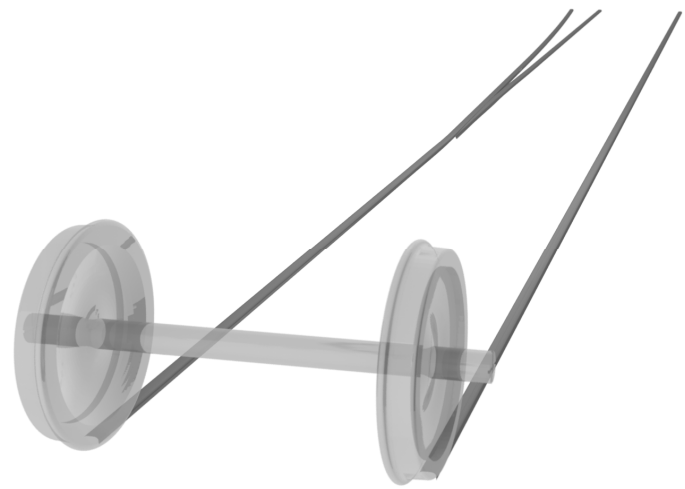

Figure 8. ANCF Quintic Plate Turnout

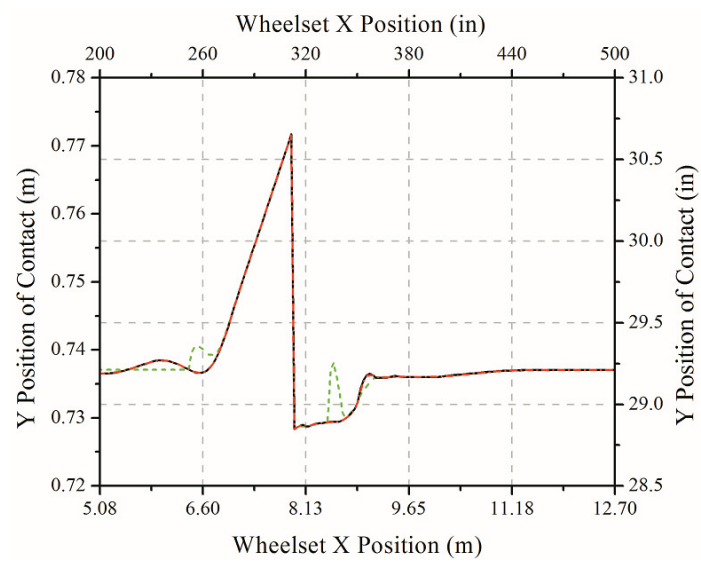

Figure 9. Y Coordinate of Contact Point on Left Rail (_ _ _ _ Linear Interpolation, _____ Quintic Plate, _ . _ . _ Cubic Plate)

interpolation of the aforementioned profiles. The ANCF thin plate meshes were generated by extracting the nodal coordinates from a B-spline surface created by the NURBS package SISL [16]. A total of 12,500 thin plate elements are used to model the left rail, while 10,000 are used to model the right rail. In this example, approximately 150 ANCF elements are used per foot of stock rail. Each rail is modeled as a separate surface with a unique parametric domain. Figure 8 shows the geometry of the turnout as produced by the quintic ANCF thin plate mesh.

5.2 Numerical Results

Among the three models, the best agreement is found in the location of the contact point. In Fig. 9, it is shown that the difference in the computed lateral position of the contact point is negligible between the cubic and quintic ANCF thin plate models while the discrepancies are more pronounced when

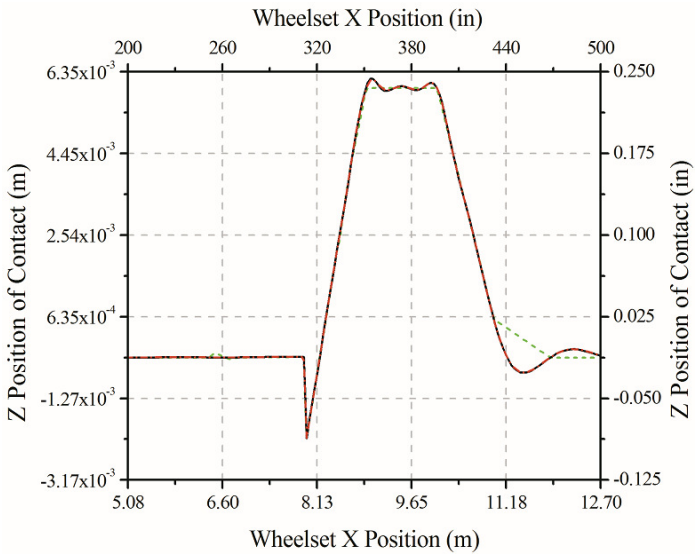

Figure 10. Z Coordinate of Contact Point on Left Rail
(_ _ _ _ Linear Interpolation, ——— Quintic Plate, _ . _ . _ Cubic Plate)

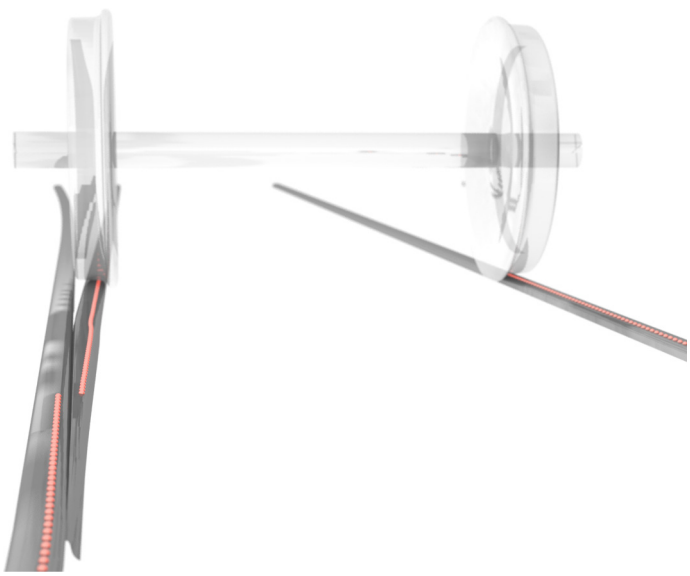

Figure 11. Trace of Contact Point along Quintic ANCF Thin Plate Turnout

compared to the linear profile interpolation method. Note that the large shift in the location of the contact point at 7.95 m (313 inches) corresponds to time at which the contact point switches from the stock rail to the switch point. A similar phenomenon can be seen in the plot of the vertical position of the contact point shown in Fig. 10. There is a small vertical shift downward as the contact point transitions from the stock rail to the switch point. Following this, the contact point shifts vertically by 0.635 cm (0.25 in) as per the design of the switch point which includes this elevation increase. It is also important to note the linear nature of the change in the vertical position of the contact point in the case of the direct profile interpolation

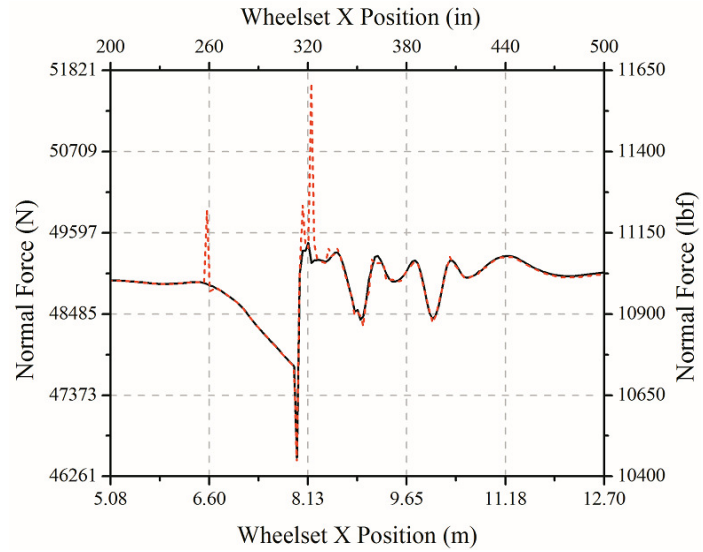

Figure 12. Normal Force at Left Contact Cubic Plate Vs. Quintic Plate
(_ _ _ _ Cubic Plate, ——— Quintic Plate)

method. Recall that linear interpolation is used in the longitudinal interpolation between any 2 profiles, consequently this leads to a linear change in the height of the profile along the rail space curve. This phenomenon is less pronounced in the lateral shift as the individual profiles are described with cubic splines. Figure 11 shows the trace of the contact points along the left rail in the proximity of the switch point. Here the cause for the lateral shift is more pronounced: the contact point shifts laterally to follow the stock rail until such a time that the primary contact point transitions from the stock rail to the switch point.

The difference between the three examples is much more pronounced in the normal contact forces. In Fig. 5, a comparison was shown for the normal contact force at the left wheel/rail interface between the direct linear interpolation method and the quintic ANCF thin plate mesh. Here it was seen clearly that the linear interpolation method produced fictitious spikes in the forces which is certainly an undesirable and unrealistic feature. However, the trend line of the linear interpolation method follows the same path as the quintic plate between these fictitious spikes. The contact forces are far more similar when the cubic and quintic plates are compared as is shown in Fig. 12. However, it is clear that some small fictitious force spikes are still predicted in the case of the cubic ANCF thin plate.

It is also important to note that the linear interpolation method required less CPU time than the ANCF methods in a serial program run on a personal computer. The cubic ANCF method required 7% more CPU time than the linear interpolation method while the quintic ANCF method required 24% more CPU time. Considering that CPU time is not penalized too greatly for the quintic ANCF method, the improved accuracy provided by this method suggests that it

would be a better choice than the other two methods in the case in which minimal CPU time for the application is not critical.

6. CONCLUSIONS

In this investigation, three different methods that may be used to define variable cross-sectional profile rail surfaces are discussed. In the first method, a linear interpolation between two profiles is used to define the surface between them. As a consequence, fictitious spikes in the contact forces are produced due to first and second order spatial derivative discontinuities which are unavoidable with this method. In the second method, a surface mesh is produced using a collection of cubic ANCF thin plate elements. This method shows marked improvement over the direct profile interpolation method, however some small fictitious spikes in the contact forces are predicted due to second order derivative discontinuities at the element boundaries. In the third method, a surface mesh is produced using a series of the newly developed quintic ANCF thin plate elements. This element has natural continuity in a mesh and as a result does not produce fictitious spikes in the forces due to spatial derivative discontinuities when used in combination with ECF-A. It was demonstrated that the linear interpolation method produces reasonable accuracy in predicting the location of the contact point. For such analyses that are not highly concerned with the contact forces, this method is ideal due to the simplicity of model creation. The cubic ANCF thin plate model produces nearly identical results at the position level when compared with the quintic ANCF thin plate model; the only discrepancy is related to some small fictitious spikes in the normal contact forces. Taking into consideration that model construction and implementation is nearly identical for the two types of ANCF thin plate elements, it is advisable to choose the quintic plate in place of the cubic plate as the increased accuracy in the force prediction outweighs the slight increase in the number of nodal coordinates when the quintic plate is chosen. It has also been shown in the literature that a linear transformation may be used to convert this quintic plate element to a quintic Bezier patch. With this procedure, one may easily develop a procedure to convert virtual prototyping, profile curve, or 3D surface scanning data to the rail surface geometry used in the contact evaluation procedures used in vehicle/track interaction simulations with little loss of geometric accuracy.

7. ACKNOWLEDGMENTS

This work was supported by the U.S. Department of Transportation NURail Center and in part by the Federal Railroad Administration. This support is gratefully acknowledged. The authors would also like to thank Cleveland Track Materials (CTM) for providing the geometric data and advice for the numerical example.

8. REFERENCES

1. Alfi, S. and Bruni, S., 2009. "Mathematical Modelling of Train-Turnout Interaction", *Vehicle System Dynamics*, Vol. 47, No 5, 551–574.
2. Cole, D. M., and Newman, P. N., 2006. "Using Laser Range Data for 3D SLAM in Outdoor Environments." *Proceedings of the IEEE International Conference on Robotics and Automation*, Orlando, Florida, USA, May 15-19.
3. Gálvez, A. and Iglesias, A., 2010. "Particle Swarm Optimization for Non-Uniform Rational B-Spline Surface Reconstruction From Clouds of 3D Data Points", *Information Sciences*, Vol. 192, 174-192, DOI:10.1016/j.ins.2010.11.007.
4. Hamper, M. B., Wei, C., Shabana, A. A., 2013. "Use of ANCF Surface Geometry in Rigid Body Contact Problems", Technical Report MBS2013-4-UIC, Department of Mechanical Engineering, University of Illinois at Chicago.
5. Hieu, L. C., Zlatov, N., Sloten, J. V., Bohez, E., Khanh, L., Binh, P. H., Oris, P., Toshev, Y., 2005. "Medical Rapid Prototyping Applications and Methods", *Assembly Automation*, Vol. 25, No 4, 284 - 292.
6. Kassa, E., Andersson, C., and Nielsen, J. C. O., 2006. "Simulation of Dynamic Interaction Between Train and Railway Turnout", *Vehicle System Dynamics*, Vol. 44, No 3, 247–258.
7. Kassa, E., Nielsen, J. C. O., 2008. "Dynamic Interaction Between Train and Railway Turnout: Full-Scale Field Test and Validation of Simulation Models", *Vehicle System Dynamics*, Vol. 46, Supplement, 521-534.
8. Lan, P. and Shabana, A. A., 2010. "Integration of B-spline Geometry and ANCF Finite Element Analysis", *Nonlinear Dynamics*, Vol. 61, 193-206.
9. Mikkola, A., Shabana, A. A., Sanchez-Rebollo, C., and Jimenez-Octavio, J. R., 2012. "Comparison Between ANCF and B-Spline Surfaces", *Multibody System Dynamics, 1-20,* DOI 10.1007/s11044-013-9353-z.
10. Piegl, L. and Tiller, W., 1997. *The NURBS Book*, 2nd Edition, Springer, New York.
11. Schupp, G., Weidemann, C., and Mauer, L., 2004. "Modelling the Contact Between Wheel and Rail Within Multibody System Simulation", *Vehicle System Dynamics*, Vol. 41, No 5, 349–364.
12. Shabana, A. A., Zaazaa, K. E., and Sugiyama, H., 2008. *Railroad Vehicle Dynamics: A Computational Approach*, CRC Press, New York, USA.
13. Shabana, A. A., 2010. *Computational Dynamics*, 3rd ed., John Wiley & Sons, Chichester, West Sussex.
14. Shabana, A. A., 2012. *Computational Continuum Mechanics*, 2nd EditionCambridge.
15. Sinokrot, T., Nakhaeinejad, M., and Shabana, A. A., 2008. "A Velocity Transformation Method for the Nonlinear Dynamic Simulation of Railroad Vehicle Systems",

Nonlinear Dynamics, Vol. 51, 289-307.
16. SINTEF ICT: Applied Mathematics, 2005. *SISL: The SINTEF Spline Library Reference Manual*, Version 4.4. http://www.sintef.no/upload/IKT/9011/geometri/sisl/manual.pdf.
17. Slob, S., Hack, R., 2004. "3D Terrestrial Laser Scanning as a New Field Measurement and Monitoring Technique", *Lecture Notes in Earth Sciences*, Vol. 104, 179-189.
18. Sugiyama, H., Tanii, Y., and Matsumura, R., 2011. "Analysis of Wheel/Rail Contact Geometry on Railroad Turnout Using Longitudinal Interpolation of Rail Profiles", *Journal of Computational and Nonlinear Dynamics*, Vol. 6, Issue 2, Technical Briefs, DOI: 10.1115/1.4002342.
19. Wan, C., Markine, V. L., and Shevtsov, I. Y., 2013. "Analysis of Train/Turnout Vertical Interaction Using a Fast Numerical Model and Validation of That Model", *Proceedings of the Institution of Mechanical Engineers, Part F: Journal of Rail and Rapid Transit*, DOI: 10.1177/0954409713489118.